

# Spatio-temporal evolution of a pulsed chlorine discharge

Vikas Midha<sup>†</sup> and Demetre J Economou

Plasma Processing Laboratory, Department of Chemical Engineering, University of Houston, Houston, TX 77204-4792, USA

Received 21 June 1999, in final form 22 December 1999

**Abstract.** A one-dimensional fluid model of a pulsed (square-wave power modulated) chlorine discharge was developed in order to study the spatiotemporal evolution of species densities and electron temperatures for various pressures, powers, pulsing frequencies and duty ratios. Simulation results show spontaneous separation of the plasma into an ion–ion core and an electron–ion edge during the power ‘on’ (active glow) fraction of the cycle. A transition from an electron-dominated plasma to an ion–ion plasma occurs during the power ‘off’ (afterglow) fraction of the cycle, under the conditions examined. The formation of an ion–ion plasma is favoured at lower power levels, higher pressures, and lower duty ratios. A minimum afterglow time is required for an ion–ion plasma to form and the negative ions to reach the walls. Increasing the afterglow period increases the fraction of time an ion–ion plasma is sustained in the reactor. The evolution of negative ion density profiles is especially complex due to the formation of self-sharpening fronts during power ‘on’ and subsequent back-propagation of the fronts during the power ‘off’ stage of the pulse. When possible, simulation results are compared to reported experimental data. In general, good agreement is obtained, except that the measured dependence of electron density on pulse period and duty ratio is more complex than predicted.

## 1. Introduction

Low-pressure, high-density plasmas are widely used in semiconductor processing for the fabrication of submicrometer devices. Recently, pulsed-power operation (in which the input power is repeatedly turned on and off) has emerged as a promising technique for improving the etching characteristics of electronegative discharges. Experiments with pulsed chlorine discharges show suppressed formation of anomalous etch profiles (e.g. notching) during poly-Si etching and reduced charging damage of the gate insulator [1–3]. This improvement in the etching characteristics of pulsed electronegative discharges compared to conventional continuous wave (CW) operation has been attributed to the role of negative ions.

Although a significant number of negative ions may be present in electronegative discharges, the flux of these ions to the wafer surface is essentially zero under CW operation. The wafer is bombarded only by electrons and positive ions. Since electrons are at a higher temperature and are much lighter than positive ions, the flux of electrons is mainly isotropic while the flux of the positive ions is anisotropic. This difference in fluxes can cause a localized build up of negative charge on the insulating side walls of a trench and a positive charge at the bottom surface. The electric fields established by this localized charging are believed to deflect oncoming positive

ions and cause etch profile distortions on the sides of narrow trenches [4–6].

In the case of pulsed discharges, however, negative ions replace the electrons as the dominant negative-charge carrier sometime in the afterglow or the power ‘off’ stage of the pulse. Since the temperature and mass of negative ions are comparable to those of positive ions, the flux of negative ions and positive ions will be equally anisotropic in nature. A negative-ion flux in the afterglow of a pulsed discharge, therefore, should help alleviate some of the problems of charging and notching associated with CW discharges. Ahn *et al* [2] suggested the concept of negative-ion assisted etching by applying a low-frequency bias (600 kHz) in the afterglow of a pulsed chlorine discharge to achieve significant reduction in notching damage compared to the case of CW operation.

Pulsed plasmas have also been shown to offer other important advantages, including: (a) improved etch selectivity by modifying the ratio of chemical species present in the plasma [7], (b) improved etch or deposition rate (for the same time-averaged power) compared to CW discharges [8], (c) reduced dust generation in the plasma [9] and (d) improved etch or deposition uniformity [10].

In order to further improve our understanding of pulsed plasmas, it becomes important to model the spatio-temporal evolution of negative ions in pulsed discharges. Existing modeling studies on pulsed operation of electronegative discharges, are mostly limited to zero-dimensional (0D) or

<sup>†</sup> Present address: General Electric-CRD, Schenectady, NY 12065, USA.

‘global’ models [11, 12]. Meyyappan [11] modeled pulsed chlorine and SF<sub>6</sub> discharges under low-pressure and high-power conditions in which the electron density did not decay sufficiently to extract a negative-ion flux out from the plasma. Ashida and Lieberman [12] showed that extraction of negative ions becomes possible only when the sheath voltage or electrostatic fields collapse in the afterglow due to thermalization and loss of electrons. Once the electrons are lost, negative-ion flux to the walls increases to become equal to the total positive-ion flux. They also showed that the coefficient for recombination of Cl radicals on the reactor walls played an important role in determining the extent of dissociation of Cl<sub>2</sub> molecules in the plasma. The neutral composition, in turn, affected the rate of decay of electrons and the evolution of negative ions in the afterglow.

In this paper, a one-dimensional (1D) fluid model for the spatio-temporal evolution of an inductively coupled pulsed chlorine discharge is developed. The model is used to demonstrate that significant changes in the spatial distribution of the negative-ion density occur during different stages of a pulse which cannot be captured by 0D models. The critical transition from an electron–ion plasma in the active glow to a negative-ion dominated or *ion–ion plasma* in the afterglow is captured, which determines the time it becomes possible to extract negative-ions out from the plasma. The evolution of the negative-ion flux from the plasma is studied as a function of the operating parameters of the pulsed discharge, i.e. power input, pressure, duty ratio and pulse period. When possible, simulation results are compared with experimental data reported in the literature. A 1D simulation of a pulsed argon discharge was reported in [13], while capacitively coupled pulsed discharges in CF<sub>4</sub> and Cl<sub>2</sub>–He were studied in [14].

## 2. Model development

The fluid approach is adopted to model the pulsed operation of inductively coupled chlorine discharges. Details on the formulation of the fluid equations are described in the literature [15] and only some of the major assumptions and key aspects relevant to pulsed discharges are discussed here. The fluid model used for the simulations consists of the following set of equations.

### 2.1. Electron energy balance

A Maxwellian electron energy distribution is assumed and an electron energy balance is constructed in terms of the electron temperature  $T_e$ :

$$\frac{\partial}{\partial t} \left( \frac{3}{2} n_e T_e \right) = -\frac{\partial q_e}{\partial x} + W - \frac{3}{2} \nu_m \delta n_e (T_e - T_g) - \sum_j R_j \Delta H_j \quad (1)$$

where  $q_e$  is the total electron energy flux given by heat conduction and convection:

$$q_e = \left( -K_e \frac{\partial T_e}{\partial x} + \frac{5}{2} k T_e \Gamma_e \right).$$

In equation (1),  $n_e$  is the electron density,  $\nu_m$  is the electron momentum transfer collision frequency,  $T_g$  is the

gas temperature,  $R_j$  is the rate of inelastic electron-impact collision  $j$ , and  $\Delta H_j$  is the corresponding electron energy loss/gain. In addition,  $W$  is the power input into the reactor, which is assumed to be spatially uniform and is square-wave modulated as a function of time to simulate the pulsed discharge. The input power is dissipated by energy losses to the walls and elastic and inelastic collisions. With the assumption of uniform power, the discharge is symmetric between the electrodes and the boundary conditions for equation (1) become  $q_e = 0$  at  $x = L/2$  (at the centre) and  $q_e = (\frac{5}{2} k T_e \Gamma_e)$  at  $x = L$ , where  $\Gamma_e$  is the electron flux,  $K_e$  is the thermal conductivity of the electron gas and  $k$  is the Boltzmann constant. Modulating the power density  $W$  modulates the electron temperature in equation (1). This, in turn, modulates the electron and ion densities (through the rate of ionization) and also the neutral densities (through the rate of dissociation).

### 2.2. Electron and ion continuity

For simplicity, the drift-diffusion approximation is used to approximate the electron and ion flux in the reactor. The electron continuity equation is given by

$$\frac{\partial n_e}{\partial t} = -\frac{\partial}{\partial x} \left( -\mu_e n_e E - D_e \frac{\partial n_e}{\partial x} \right) + \sum_j R_j \quad (2)$$

and the ion continuity equation (Cl<sup>+</sup>, Cl<sub>2</sub><sup>+</sup> and Cl<sup>-</sup> are considered) is given by

$$\frac{\partial n_i}{\partial t} = -\frac{\partial}{\partial x} \left( s_i \mu_i n_i E - D_i \frac{\partial n_i}{\partial x} \right) + \sum_j R_j \quad (3)$$

where  $s_i$  represents the charge of the ion species. Here  $n_i$  is the ion (positive or negative) density,  $E$  is the electrostatic field and  $\mu$  and  $D$  are the species mobility and diffusivity, respectively. The summation terms on the right-hand sides of equations (2) and (3) include all reactions that produce or destroy electrons or ions. For electrons, for example, these include ionization (both atomic and molecular chlorine), attachment and detachment. For negative ions, these include attachment, detachment and negative-ion–positive-ion recombination. Both electrons and ions are assumed to recombine at the walls so the boundary conditions  $\Gamma = 0$  at  $x = L/2$  (at the centre) and  $n \approx 0$  at  $x = L$  (the wall) are employed. Only the bulk plasma is treated here, neglecting the very thin sheath. The electron density decays significantly during the afterglow and a small but finite value of  $n_e$  is fixed at the walls to avoid singularity in equation (1). Instead of the drift-diffusion approximation, calculation of ion fluxes using the full momentum equations may be more suitable for low operating pressures in order to capture features such as the formation of double layers predicted for CW electronegative discharges [16, 17].

An ion temperature of 0.026 eV (room temperature) was assumed in this study because the ion temperature is generally unknown. However, simulations were also performed using higher ion temperatures (0.1 eV) and the conclusions of this paper remain the same.

### 2.3. Neutral transport

Neutral particle densities  $n_k$  are calculated by accounting for diffusion, reaction and flow losses through the residence time  $\tau_{res}$

$$\frac{\partial n_k}{\partial t} = -\frac{\partial}{\partial x} \left( -D_k \frac{\partial n_k}{\partial x} \right) + \sum_j R_j - \frac{n_k}{\tau_{res}}. \quad (4)$$

The Cl radical density is calculated using the boundary conditions  $\partial n_{Cl}/\partial x = 0$  at  $x = L/2$  (at the centre) and

$$-D_{Cl} \frac{\partial n_{Cl}}{\partial x} = \frac{\gamma}{4} n_{Cl} v_{Cl} - \Gamma_{Cl^+}$$

at  $x = L$  where  $\gamma$  is the recombination coefficient for Cl radicals on the electrodes,  $v_{Cl}$  is the thermal velocity of Cl radicals and  $\Gamma_{Cl^+}$  is the flux of  $Cl^+$  ions. The  $Cl_2$  density, in turn, is calculated from the Cl density and the constraint of constant total neutral density. The gas temperature is assumed to be constant at 300 K.

### 2.4. Electrostatic fields

The electrostatic fields in the plasma can be calculated self-consistently from the Poisson equation given by

$$\frac{\partial E}{\partial x} = \frac{q}{\epsilon_0} \left( \sum_i s_i n_i - n_e \right). \quad (5)$$

where  $q$  is the elementary charge and  $\epsilon_0$  is the permittivity of free space. However, the electrostatic field in the bulk plasma (outside of the sheath) can be calculated from the condition of no net current

$$\sum_i s_i \Gamma_i - \Gamma_e = 0. \quad (6)$$

By substituting the drift-diffusion approximation for the electron and ion fluxes, the following expression for the electrostatic field may be derived:

$$E = \left( \frac{\sum_i (s_i D_i \partial n_i / \partial x) - (D_e \partial n_e / \partial x)}{\sum_i \mu_i n_i + \mu_e n_e} \right) \quad (7)$$

At this point, it is instructive to examine some of the limiting cases of equation (7). For the case of one type of positive ion with diffusivity  $D_p$  and mobility  $\mu_p$  and one type of negative ion with diffusivity  $D_n$  and mobility  $\mu_n$ , equation (7) may be simplified to

$$E = \left( \frac{(D_p \partial n_p / \partial x) - (D_e \partial n_e / \partial x) - (D_n \partial n_n / \partial x)}{\mu_p n_p + \mu_e n_e + \mu_n n_n} \right) \quad (8)$$

where  $n_p$  is the positive-ion density and  $n_n$  is the negative-ion density. By invoking the assumption of quasineutrality ( $n_p = n_e + n_n$ ) in the bulk plasma, equation (8) may be simplified further to

$$E = \left( \frac{[(D_p - D_e) \partial n_e / \partial x] + [(D_p - D_n) \partial n_n / \partial x]}{(\mu_p + \mu_e) n_e + (\mu_p + \mu_n) n_n} \right). \quad (9)$$

Depending on the ratio of the negative-ion and electron densities, three different cases may be identified.

(a) *Electron-ion plasma.* If the electron density is not too small ( $n_n/n_e \ll \mu_e/(\mu_n + \mu_p)$ ) and the usual conditions of  $D_e \gg D_p, D_n$  and  $\mu_e \gg \mu_p, \mu_n$  are satisfied, equation (9) may be simplified to

$$E = \left( \frac{-D_e \partial n_e / \partial x}{\mu_e n_e} \right) = -T_e \left( \frac{\partial n_e / \partial x}{n_e} \right) \quad (10)$$

i.e. the electric field is determined by the Boltzmann equilibrium of electrons and is a function of the electron temperature  $T_e$ . The negative ions do not play a major role. This is the usual condition for weakly electronegative CW discharges and the active glow of pulsed discharges.

(b) *Intermediate case.* As the electron density decreases in the afterglow, the contribution of negative ions starts becoming significant. In this case, equation (9) simplifies to

$$E = \left[ \frac{-D_e \partial n_e / \partial x}{\mu_e n_e + (\mu_n + \mu_p) n_n} \right] \quad (11)$$

i.e. the electrostatic fields are reduced from the corresponding Boltzmann expression (equation (10)) due to the presence of negative ions. If  $\mu_p = \mu_n$ , then the electronegativity at which the contribution of negative ions starts dominating over that of electrons is given by the condition

$$\frac{n_n}{n_e} = \frac{1}{2} \frac{\mu_e}{\mu_n}. \quad (12)$$

At this stage, electrons are no longer in Boltzmann equilibrium with electron diffusion dominating over electron drift.

(c) *Ion-ion plasma.* In the limiting case where the electron density becomes negligible compared to the negative-ion density ( $n_n/n_e \gg \mu_e/(\mu_n + \mu_p)$ ), equation (9) simplifies to

$$E = \left( \frac{(D_p - D_n) \partial n_n / \partial x}{(\mu_p + \mu_n) n_n} \right) \\ E = 0 \quad \text{if } D_p = D_n. \quad (13)$$

The electrostatic fields are now determined by the negative ions and the negative-ion temperature  $T_i$ . The magnitude of the electrostatic fields in an ion-ion plasma, therefore, is considerably less than the electrostatic fields in a conventional electron-ion plasma where  $T_e \gg T_i$ . In the limiting case of equal positive-ion and negative-ion diffusivities there are no electrostatic fields (and therefore no sheaths in an unbiased plasma) in an ion-ion plasma. Clearly, in the absence of electrostatic fields the positive ions are not accelerated to the Bohm velocity and ion flux is determined by diffusion alone.

An equivalent analysis may be conducted by substituting the expression for the electric field (equation (9)) into the electron continuity equation (equation (2)). An effective electron diffusivity  $D_{eff}$  [18] may be defined by  $\Gamma_e = (-\mu_e n_e E - (D_e \partial n_e / \partial x)) = -D_{eff} \partial n_e / \partial x$ , where

$$D_{eff} = \left( \frac{1 + 2(n_n/n_e)}{[(\mu_e/\mu_n) + 1] + 2(n_n/n_e)} \right) D_e \quad (14)$$

for the case  $\mu_n = \mu_p$ .

**Table 1.** Reaction chemistry included in the simulations [22].

No	Process	Reaction	Threshold (eV)
Electron impact reactions			
1	Dissociative excitation	$\text{Cl}_2 + e \rightarrow \text{Cl}_2^*(\text{C}^1\Pi) + e \rightarrow 2\text{Cl} + e$	3.12
	Electronic excitations (molecular)	$\text{Cl}_2 + e \rightarrow \text{Cl}_2^* + e$	
2	$\text{B}^3\Pi$		2.49
3	$2^1\Pi$ and $2^1\Sigma$		9.25
	Electronic excitations (atomic)	$\text{Cl} + e \rightarrow \text{Cl}^* + e$	
4	4s		8.90
5	4p		10.40
6	3d		10.90
7	5p		11.80
8	4d		12.00
9	5d		12.40
10	Molecular ionization	$\text{Cl}_2 + e \rightarrow \text{Cl}_2^+ + e$	11.47
11	Atomic ionization	$\text{Cl} + e \rightarrow \text{Cl}^+ + e$	12.99
13	Dissociative attachment	$\text{Cl}_2 + e \rightarrow \text{Cl}^- + \text{Cl}$	
14	Electron-ion neutralization	$e + \text{Cl}_2^+ \rightarrow 2\text{Cl}$	
15	Electron detachment	$e + \text{Cl}^- \rightarrow \text{Cl} + 2e$	3.61
16	Vibrational excitation	$\text{Cl}_2 + e \rightarrow \text{Cl}_2^* + e$	0.0689
Other reactions			
17	Ion-ion recombination	$\text{Cl}_2^+ + \text{Cl}^- \rightarrow \text{Cl}_2 + \text{Cl}$	
18	Ion-ion recombination	$\text{Cl}^+ + \text{Cl}^- \rightarrow 2\text{Cl}$	
19	Wall recombination	$2\text{Cl} + \text{wall} \rightarrow \text{Cl}_2 + \text{wall}$	

The same three cases may be identified in terms of the plasma electronegativity ( $n_n/n_e$ ),

(a) Electron-ion plasma. When the electronegativity is low  $n_n/n_e \ll \frac{1}{2}$

$$D_{eff} = \frac{\mu_n}{\mu_e} D_e = \mu_n T_e \quad (15)$$

which is the usual ambipolar diffusion coefficient for electropositive discharges.

(b) Intermediate case. As the electronegativity increases  $\frac{1}{2} < n_n/n_e < \frac{1}{2}\mu_e/\mu_n$

$$D_{eff} = \left[ 1 + 2 \left( \frac{n_n}{n_e} \right) \right] \frac{\mu_n}{\mu_e} D_e \quad (16)$$

i.e. the effective diffusivity of the electrons is enhanced by the presence of negative ions in the discharge. This is due to the corresponding reduction in electrostatic fields which would otherwise confine electrons in the plasma.

(c) Ion-ion plasma. When negative ions become the dominant negative-charge carrier in the plasma  $n_n/n_e \gg \frac{1}{2}\mu_e/\mu_n$ ,

$$D_{eff} = D_e. \quad (17)$$

i.e. the electrostatic fields collapse in the limit of an ideal ion-ion plasma and the effective diffusivity approaches the free diffusivity of electrons. The reader is referred to [19] for more details on the theoretical analysis of some limiting cases of the afterglow of electronegative discharges.

In addition to the temporal variation of the electronegativity of the discharge in the afterglow, the same analysis is valid for any spatial variation of electronegativity in the bulk plasma. As will be shown in the following sections, significant spatial variation in the negative-ion density may occur along the length of the reactor. From equations (11)

and (16), the electrostatic fields are reduced in the presence of a large negative-ion density, leading to a corresponding enhancement in the effective electron diffusivity. Alternately, the electrostatic fields are stronger in spatial locations with a low negative-ion density and the electrons are well confined. Therefore, an accurate calculation of the rate of decay of electron density and extraction of negative-ion flux requires an account of *both the spatial and the temporal* variation of the electrostatic fields in the pulsed plasma.

Calculations were also performed by solving the energy and continuity equations (equations (1)–(4)) along with Poisson equation ((equation (5)) for the electrostatic fields resolving the sharp gradients in the very thin sheath region [20]. In the afterglow, the electrostatic fields in the sheath region collapsed abruptly (several orders of magnitude within a few microseconds) after the bulk electrostatic fields collapsed due to the drop in electron temperature and the decay of electron density. Therefore, subsequent calculations were performed only for the bulk plasma by assuming quasineutrality and using the ambipolarity constraint (equation (7)) for the electrostatic fields instead of the Poisson equation. This approximation resulted in a significant reduction in the computational burden (for instance, the CPU time was reduced from several hours to a few minutes on an HP 125 MHz Unix workstation) and was adopted for all the results presented in this work.

### 3. Results and discussion

The partial differential equations of the model were discretized in space using finite-difference approximations. The resulting set of ordinary differential equations was integrated in time using an implicit ordinary differential equation integrator [21] until a periodic steady state in the spatio-temporal variation of  $T_e$ ,  $n_e$ ,  $n_{\text{Cl}_2^+}$ ,  $n_{\text{Cl}^+}$ ,  $n_{\text{Cl}^-}$ ,  $E$ ,  $\text{Cl}$

**Table 2.** Base case parameters and operating conditions.

Inter-electrode spacing	3.8 cm
Pressure	20 mTorr
Power density	$1.0 \text{ W cm}^{-3}$
Pulse period	$100 \mu\text{s}$
Duty ratio	0.5
Cl surface recombination coefficient	0.1
Ion temperature	0.026 eV
Gas temperature	300 K

**Table 3.** Characteristic time scales of physical processes (in microseconds).

Electron energy conduction	0.1
Inelastic energy dissipation	0.1
Electron (free) diffusion	0.1
Ambipolar diffusion	10
Ionization	10
Electron attachment	10
Ion-ion recombination	10
Pulse width	100
Ion (free) diffusion	1000
Neutral excitation	1000
Neutral diffusion	1000
Cl surface recombination	1000
Gas residence time	10 000

and  $\text{Cl}_2$  was attained. Table 1 summarizes the chemistry considered in the simulations [22]. The base conditions used in the simulations are given in table 2 and correspond to the experimental conditions of Hebner and Fleddermann [23].

Table 3 shows the characteristic time scales of some important physicochemical processes involved in the evolution of the pulsed chlorine discharge. For the conditions considered, power input into the plasma is expected to be balanced mainly by energy losses due to inelastic collisions. Electrons produced by ionization are lost mainly by ambipolar diffusion to the walls and dissociative attachment with  $\text{Cl}_2$  molecules. Negative ions produced by this dissociative attachment, are confined by the ambipolar fields and are lost by volume recombination with positive ions. Cl radicals are produced mainly by electron-impact dissociation of  $\text{Cl}_2$  molecules and are lost mainly by diffusion and recombination at the walls. Since the gas residence time is significantly greater than neutral diffusion and the surface recombination time, gas flow is not expected to be important under these conditions.

Based on a comparison of the time scales of dominant processes, the electron temperature evolution is expected to respond at the fastest time scale ( $0.1 \mu\text{s}$ ) followed by electron and ion densities ( $10 \mu\text{s}$ ) followed by neutral densities ( $1000 \mu\text{s}$ ). The time scale for electron and ion density evolution is shorter than typical values of the pulse period. Therefore, the electron and ion densities are expected to respond to the instantaneous value of the power. The response time of neutrals, however, is much longer than typical values of the pulse period. The neutral composition, therefore, is expected to respond only to the time-averaged value of the power and eventually reach a weakly-modulated, periodic steady state. In all figures shown below, lengths of 1.9 cm and 3.8 cm correspond to the centreline and the right-hand-side wall of the 1D parallel plate system, respectively.

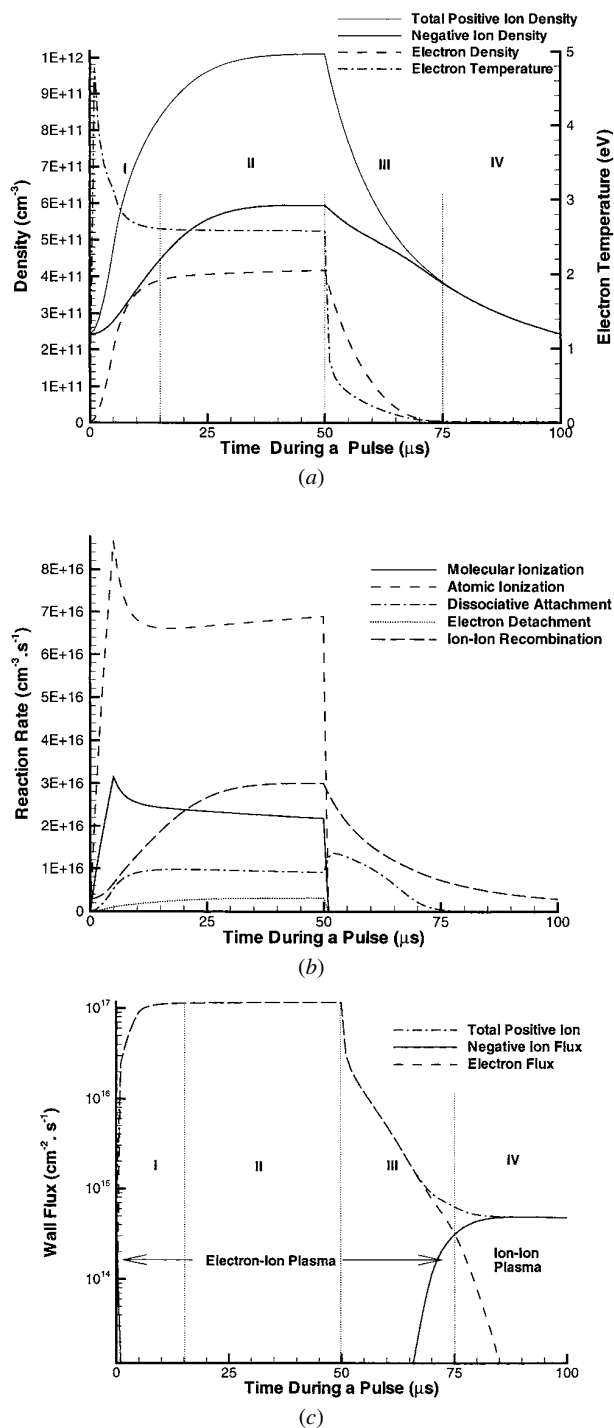


**Figure 1.** For the base case conditions (table 2): (a) evolution of electron temperature and plasma density, (b) rates of chemical reactions at the centre of the reactor; and (c) evolution of wall flux of different species.

Figure 1(a) shows the evolution of species densities and electron temperature at the *centre* of the reactor once a periodic steady-state is achieved. The period 0–50  $\mu\text{s}$  represents the time power is 'on' (active glow) while the period 50–100  $\mu\text{s}$  represents the time power is 'off' (afterglow) during a pulse. For convenience, the overall evolution during a pulse is divided into four different regimes: (I) early active glow, (II) late active glow, (III) early afterglow

and (IV) late afterglow. The overall trends shown in figure 1(a) are in good agreement with experimental results reported in the literature [23–25]. The electron temperature shows the formation of a sharp spike as soon as the power is switched ‘on’, and then drops abruptly in the afterglow. The electron density shows a large variation of several orders of magnitude in the active glow and the afterglow while the negative ions are considerably less modulated. The plasma is weakly electronegative in the active glow and then becomes increasingly electronegative in the afterglow. The electron density decays rapidly in the afterglow to a point when it becomes negligible compared to the negative ion density and an ion–ion plasma is formed (equation (17) is satisfied).

As discussed earlier, several physicochemical processes with comparable time scales are responsible for the evolution of the pulsed chlorine discharge. To aid understanding, figure 1(b) shows the rates of the important chemical reactions at the centre of the discharge. Figure 1(c) shows the flux of the various species at the wall of the reactor as a function of time during a pulse. Each of the four stages (I–IV) during a pulse is discussed separately below.

### 3.1. Early active glow (0–15 $\mu\text{s}$ )

Since the results represent a periodic steady state, the initial condition of the plasma at the beginning of the active glow also corresponds to the final condition at the end of the afterglow. For the base set of parameters (table 2), this condition consists of an ion–ion plasma without a significant number of electrons. Once the power is switched ‘on’, the electron temperature attains a sharp spike, while the electron density continuously increases to attain a quasi-steady-state value at the end of the early active glow (figure 1(a)).

Initially, the electrostatic field is weak in the absence of a significant number of electrons; it is determined by the negative ions (equation (13)). Therefore, any electrons that are generated by ionization are able to diffuse freely to the walls. When power is deposited in this small number of electrons, the electron temperature rises sharply. The electron temperature increases till production of electrons by ionization eventually overcomes diffusion losses to the walls and the electron density increases as a function of time. Once a sufficient number of electrons is generated, electron energy is dissipated by inelastic collisions and the electron temperature begins to drop.

The spike in electron temperature in the early stages of the active glow characterizes the final condition of the plasma at the end of the afterglow; a large spike indicates that effectively all electrons were lost in the afterglow and an ion–ion plasma was formed, whereas no spike indicates that a significant number of electrons remained in the afterglow. This trend has been observed experimentally by Malyshev *et al* [24, 25] and will be discussed again in the following sections. A similar spike in electron temperature is predicted by Ashida and Lieberman [12] when the electron density decays significantly, whereas no spike is reported by Meyyappan [11] when the electron density is weakly modulated.

Figure 1(a) shows that there is an overall increase in the central negative ion density in the early active glow. Although dissociative attachment is slower than ion recombination

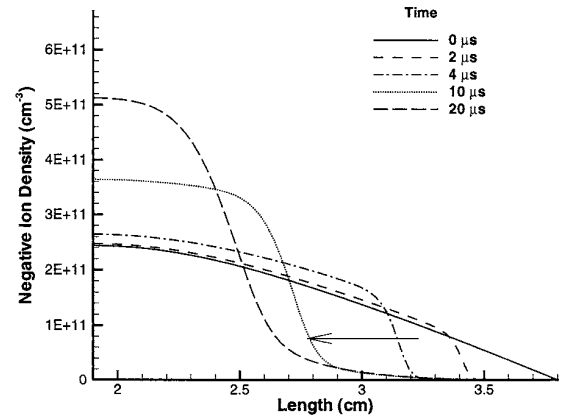


**Figure 2.** Spatial evolution of negative-ion density in the early active glow (base case conditions, table 2).

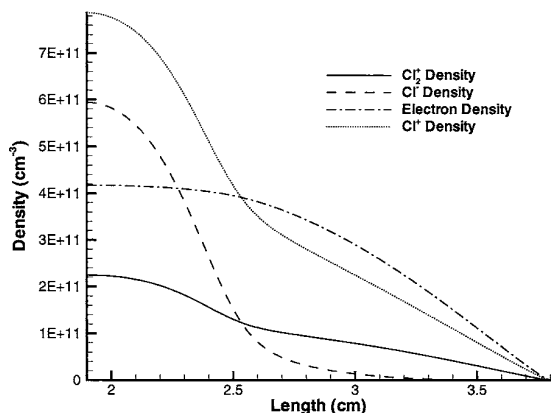
(see figure 1(b)), an increase in negative ion-density occurs. This indicates that there is a significant flux of negative-ions towards the centre of the discharge arising from a change in the spatial distribution of negative ions.

Figure 2 shows the spatial evolution of the negative ion density in the early active glow. By the end of the preceding pulse, negative ions have diffused to the walls in the absence of significant electrostatic fields. As the electrostatic fields rise with electron temperature, negative ions are rapidly squeezed towards the centre of the plasma. Since the electric field is higher at the edges as compared to the centre of the plasma (where the negative ion density is maximum), the front of the negative ions sharpens as a function of time in the early active glow. This self-sharpening of the front proceeds until ion diffusion across the front begins to balance ion drift due to electrostatic fields. As a result of this entrapment of the negative ions in the core of the discharge, the flux of the negative ions at the walls quickly drops to zero in the early stages of the active glow (figure 1(c)). The formation of sharp spatial fronts in the transient evolution of the negative ions was analysed theoretically by Kaganovich and Tsendin [26] (see also [19]).

### 3.2. Late active glow (15–50 $\mu\text{s}$ )

Both the electron temperature and density reach a quasi-plateau changing only slowly in the late active glow. This quasi-steady state represents a balance between the heating of electrons by power input and the dissipation of electron energy mainly by inelastic collisions. Most of this energy dissipation occurs through neutral excitations. A small fraction of electron energy is dissipated through ionization in the late stages of the active glow. Similarly, the production of electrons by ionization is balanced by loss due to attachment and ambipolar diffusion to the walls. Figure 1(b) shows that atomic ionization dominates over molecular ionization, suggesting that  $\text{Cl}^+$  is the dominant positive ion in the discharge for the base case conditions.

The plateau in electron temperature and density does not, however, signify that the plasma has reached a steady state in the late stages of the active glow. In order to reach a steady state, the neutral composition must acquire a steady state at the instantaneous or peak value of input power.



**Figure 3.** Spatial distribution of electron and ion densities at the end of the active glow (base case conditions, table 2,  $t = 50 \mu\text{s}$ ).

Since the response time of neutrals is several milliseconds, the neutral composition responds only to the time-averaged value of power and is still far from a steady state in the late active glow. The characteristic difference between the active glow of pulsed discharges and continuous wave discharges, therefore, is that electron and ion densities correspond to the peak power level while the neutral composition corresponds to the time-averaged power level.

The transient nature of the neutral composition in the late active glow is evident from figures 1(a) and 1(b). Figure 1(b) shows that the rate of atomic ionization increases in the late active glow, while the rate of molecular ionization decreases as the  $\text{Cl}_2$  molecules are slowly dissociated. Similarly, the rate of attachment decreases slightly in the late active glow. Electron energy dissipation by Cl excitations increases while dissipation by  $\text{Cl}_2$  excitations decreases (not shown).

Figure 3 shows the presence of two distinct spatial regions in the bulk plasma at the end of the active glow:

- (1) an electronegative core (for length less than  $\sim 3$  cm) where almost all negative ions are trapped,
- (2) an electropositive edge plasma where negative ions are absent.

Negative ions are produced by dissociative attachment throughout the length of the reactor. Due to the presence of electrostatic fields, however, negative ions produced in the edge region are continuously squeezed into the core. As a result of this entrapment, there is no negative-ion flux to the walls in the late active glow. Production of negative ions by attachment is balanced by ion-ion recombination which is limited only to the core region of the discharge. Since the length of the core is smaller than the length of the discharge, the rate of recombination at the centre in figure 1(b) is higher than the rate of dissociative attachment. The magnitude of the electrostatic fields is significantly reduced in the electronegative core, resulting in an enhancement in the effective diffusivity there (equations (11) and (16)). The profile of the electron density, therefore, is flattened in the electronegative core (figure 3). In the electropositive edge, however, the effective diffusivity of the electrons approaches the ambipolar diffusivity of electropositive discharges (equation (15)) due to lack of negative ions. This separation of the plasma into an

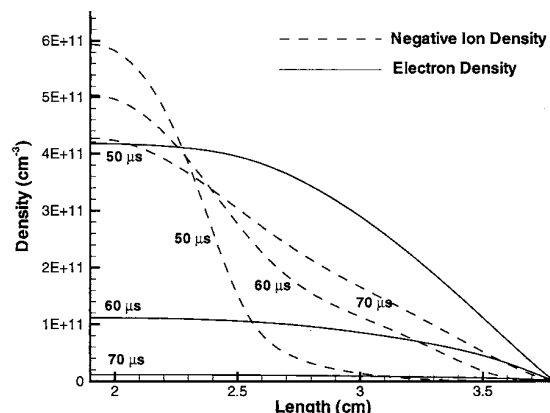


**Figure 4.** Spatial evolution of negative-ion and electron densities in the early afterglow (base case conditions, table 2).

electronegative core and electropositive edge is similar to the structure of CW electronegative discharges which have been analysed extensively in the literature [26–28].

### 3.3. Early afterglow (50–75 $\mu\text{s}$ )

The quasi-steady state attained in the active glow ensures that the power input into the electrons is balanced by inelastic collisions. Once the power is switched off, there is only a loss of electron energy by collisions and the electron temperature plummets within the first few microseconds. Eventually, however, the rate of these inelastic collisions decreases at the lower electron temperatures and the temperature decays at a lower rate in the early afterglow (figure 1(a)).

While the rate coefficients of most electron impact reactions decrease as the electron temperature drops, the rate coefficient of dissociative attachment increases in the afterglow [29]. This enhancement in the rate of attachment results in a faster rate of decay of electron density in the early afterglow. The overall rate of attachment, however, goes through a maximum as a function of time in the afterglow (figure 1(b)); the attachment rate increases initially at the lower electron temperatures and then decreases as the electron density becomes too low.

An integration of the rate of attachment with respect to time in figure 1(b) shows that a significant fraction (30%) of the initial electron density is lost by dissociative attachment in the afterglow, while the rest is lost by diffusion to the walls. The loss of electrons by attachment corresponds to an increase in the negative-ion density by about 20%. The negative-ion density at the centre of the discharge, however, uniformly decreases in the afterglow (figure 1(a)). This indicates that there is a considerable flux of negative ions out of the centre, and thus a change in the spatial distribution of negative ions.

Figure 4 shows the spatial evolution of the negative ion density in the early stages of the afterglow. Two mechanisms are responsible for the change in spatial profiles of negative ions.

- (1) The electrostatic fields which trap negative ions in the core of the reactor weaken as the electron temperature drops in the afterglow (equation (10)). The sharp front

of negative ions formed in the active glow spreads in the afterglow as negative ions diffuse towards the walls.

- (2) New negative ions are generated throughout the discharge as a result of the enhanced rate of attachment in the afterglow. Negative ions formed in the electropositive periphery are not trapped as much due to the weaker electrostatic fields in the afterglow. As a result, the electropositive periphery region shrinks while the electronegative core expands towards the walls.

It may be noted from figure 1(c), however, that the negative-ion flux to the walls is still negligible compared to the electron flux in most of the early afterglow. The electrostatic field is reduced in the electronegative core due to the presence of negative ions (equation (11)), but is still significant in the electropositive edge region. The electrostatic field due to a small number of electrons is enough to trap negative ions in the discharge. An accurate prediction of the evolution of the negative-ion flux requires an account of how these fields change in both space and time with negative-ion fronts. The electron (and positive-ion) flux in figure 1(c) decays rapidly within the first few microseconds and at a lower rate thereafter due to the dependence of the effective diffusivity of electrons on electron temperature (equation (15)). The magnitude of the electron flux decreases monotonically by about two orders of magnitude with the decaying electron density in the afterglow. Ashida and Lieberman [12] report a non-monotonic variation in the electron and positive-ion flux at this stage of the afterglow and attribute it to a rise in the 'h factor' which relates bulk positive-ion density to the positive-ion density at the sheath presheath boundary in their 0D model. This behaviour was not observed in our spatially-resolved simulations.

### 3.4. Late afterglow (75–100 $\mu$ s)

Electrons are lost rapidly in the early afterglow by ambipolar diffusion to the walls and dissociative attachment while negative ions are still trapped in the reactor. As can be deduced from Equation 12, once the electron density  $n_e$  is less than  $\frac{1}{2}(\mu_i/\mu_e)n_n$  throughout the length of the reactor, negative ions become the dominant negative-charge carrier in the plasma. The electric field is now determined by negative ions instead of electrons and there is an abrupt transition from an electron-dominated plasma to an ion–ion plasma. As discussed earlier, the ion–ion plasma is characterized by weak electrostatic fields and a diffusive flux of negative ions to the walls. In figure 1(c), the transition from an electron–ion plasma to an ion–ion plasma is characterized by the electron flux becoming equal to the negative ion flux at the walls ( $t = 75 \mu$ s). The positive-ion flux, which initially overlaps with the electron flux in the early afterglow becomes equal to the negative-ion flux in the late afterglow. Experimental results reported by Smith *et al* [30] in the afterglow of an oxygen plasma show similar behaviour: the negative-ion flux was negligible in the early afterglow and abruptly increased by several orders of magnitude to become equal to the positive-ion flux in the late afterglow.

After the transition to an ion–ion plasma, electrons are no longer confined in the plasma and are lost at a faster rate that eventually approaches the limit of free diffusion of electrons

to the walls in the absence of electrostatic fields. The positive-ion and negative-ion densities decay together much more slowly due to ion–ion recombination and diffusion losses to the walls. The peak magnitude of the negative-ion flux is about two orders of magnitude less than the electron flux in the active glow. This corresponds, roughly, to the ratio of the ambipolar diffusion coefficient to the ion diffusion coefficient, or, the ratio of electron temperature in the active glow ( $\sim 3$  eV) to the ion temperature ( $\sim 0.03$  eV). This is significantly different from the results of Ashida and Lieberman [12] which show the peak negative-ion flux to be about 25% of the electron flux at the end of the active glow. This ratio roughly corresponds to the ratio of the Bohm velocity evaluated at the electron temperature in the active glow to the Bohm velocity evaluated at the ion temperature used in their simulations. However, the appropriate limit of the negative-ion flux in a collisional ion–ion plasma is the diffusive flux of negative (and positive) ions, not the Bohm flux of positive ions evaluated at the ion temperature.

Processing with ion–ion plasmas at the late afterglow offers unique possibilities. Preliminary calculations (which included the Poisson equation and resolved the sheaths) show that application of a radio-frequency bias results in bombardment of the walls by positive and negative ions alternately [20]. As demonstrated experimentally by Ahn *et al* [2], this has significant potential to reduce charging and notching effects associated with conventional CW electron–ion plasma processing.

In order to facilitate plasma ignition when power was turned back on, the electron density was not allowed to drop in the afterglow beyond a cut-off value of  $10^8 \text{ cm}^{-3}$ . It was verified that the simulation results are not altered by the choice of this cut-off value, except for a slight effect on the evolution of  $T_e$  in the first  $2 \mu$ s after power on. With this cut-off value of electron density, the ratio of the negative-ion density to the electron density in the late afterglow was 1000, much higher than a value of a few hundred, above which electrons have no effect on the plasma dynamics. A similar procedure (use of a cut-off value for electron density) was used by Ashida and Lieberman [12].

### 3.5. Negative-ion density and comparison with experiments

Figure 1(a) shows that the negative-ion density at the centre of the reactor uniformly increases in the active glow and then decreases in the afterglow. Experimental results for comparable conditions [23], however, show that after an initial increase, the negative-ion density decreases in the active glow and then increases again to form a peak in the afterglow. This difference in behaviour may be attributed to the 1D nature of the model. An accurate description of the power distribution in the reactor would require a 2D model in both the axial and radial coordinates. However, since power will be localized near the coils at the upper electrode of the GEC reactor, the profiles are not expected to be axially symmetric between the electrodes. Therefore, some insight may be gained by examining the evolution of the negative-ion density at points other than the centre of the reactor.

Figure 5 shows the evolution of negative-ion densities at three different positions. The time dependence of the

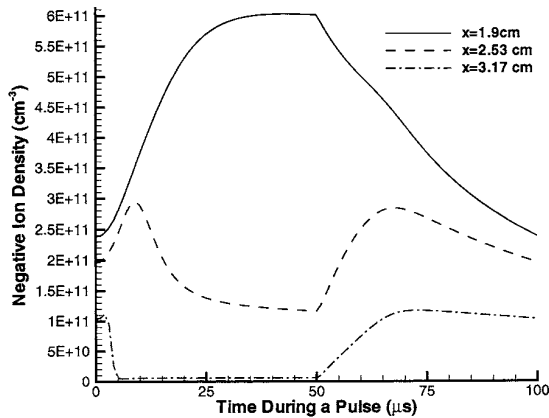


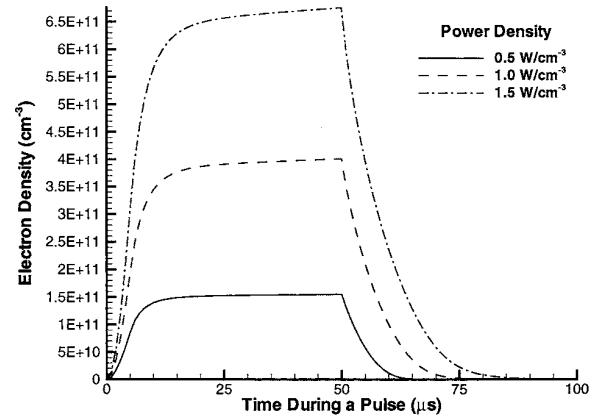
**Figure 5.** Evolution of negative-ion density at different spatial locations (base case conditions, table 2).

negative-ion density at the off-centre location at  $x = 2.53$  cm shows much better agreement with experimental data. The negative-ion density increases in the early active glow as negative ions are squeezed from the edge towards this point (figure 2,  $t = 2, 4$  and  $10 \mu\text{s}$ ). The negative-ion density then decreases as the front of negative ions passes this point towards a more central location (figure 2,  $t = 20 \mu\text{s}$ ). The reverse process occurs in the afterglow as the electronegative core expands and the front of negative ions moves back towards the walls (figure 4). The negative-ion density increases as the front passes this point and eventually decays due to ion-ion recombination and diffusion losses to the walls.

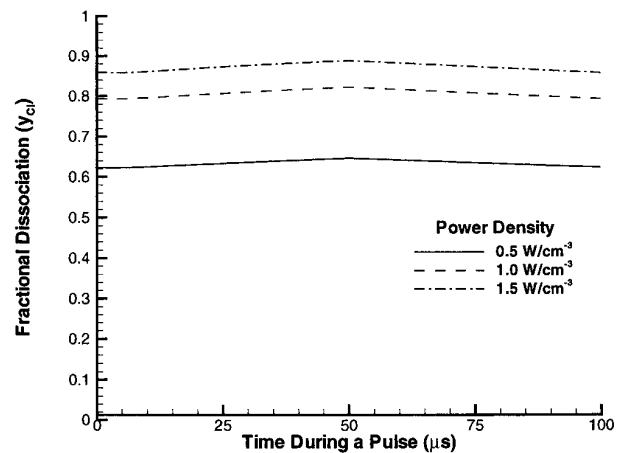
The results in figure 5 demonstrate that a significant variation in the spatial distribution of negative ions occurs during the pulse. The peak of the negative-ion density may be off-centre in the active glow due to localized power deposition and non-uniform neutral densities in the reactor (e.g. see simulated negative-ion density profiles for a CW chlorine discharge in [22]). Measurement of negative-ion density at the reactor centre only may lead to a significant underestimation of the peak electronegativity of the plasma. Similarly, multidimensional models for pulsed discharges are required to accurately capture the evolution of negative-ion profiles in complex reactor geometries.

### 3.6. Effect of operating parameters

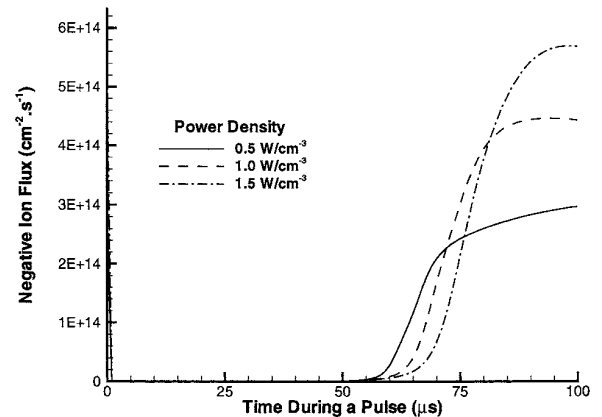
From the previous discussion, it becomes apparent that the time at which negative ions can be extracted from the plasma (figure 1(c)) is related to the time required for the electron density to decay significantly. The rate of electron decay is dependent on the rate of diffusion losses to the walls and the rate of attachment of electrons to  $\text{Cl}_2$  molecules. From equations (14)–(17), the effective diffusivity of the electrons is a function of pressure, electron temperature and plasma electronegativity. Due to its dependence on electronegativity, the effective diffusivity of electrons is spatially non-uniform and evolves in time with the changing negative-ion density profiles. Similarly, the rate of attachment of electrons is a function of electron temperature and the  $\text{Cl}_2$  density in the plasma. In the following sections, the effect of varying key



(a)



(b)



(c)

**Figure 6.** Effect of peak power on the evolution of: (a) the electron density, (b) the  $\text{Cl}$  mole fraction and (c) the negative-ion flux at the walls. The other conditions are at their base values (table 2).

operating parameters on the evolution of plasma properties and negative-ion flux is examined.

**3.6.1. Peak input power.** As in the case of CW discharges, the peak input power does not affect the electron temperature significantly, but changes the electron density in the active glow. As the peak value of power in the active

glow is increased, more electrons are required to dissipate the additional electron energy through inelastic collisions. Therefore, the quasi-steady value of electron density during the active glow steadily increases with increasing peak power (figure 6(a)). This trend is well known for CW discharges and has also been observed experimentally for pulsed chlorine discharges [23]. Both experimental and model results show that the increase in the plateau value of the electron density is not linear with power input. This suggests that the neutral composition also changes as the peak power level is changed.

In the transient phase of plasma ignition, when the neutral composition is yet to acquire a periodic steady state, each additional pulse leads to accumulation of Cl radicals and a corresponding depletion of Cl<sub>2</sub> molecules. The net production of Cl in each successive pulse diminishes as the Cl<sub>2</sub> molecules are depleted. Eventually, a periodic steady state is reached in which generation of Cl is balanced by loss of Cl within the pulse by diffusion and wall recombination. Increasing the power input level results in higher electron densities, which in turn favour more dissociation of Cl<sub>2</sub> molecules into Cl radicals. Therefore, the time-averaged value of the Cl density in the periodic steady state increases monotonically as the peak power level is increased (figure 6(b)).

As discussed earlier, the input power is balanced mainly by excitation of neutrals in the late active glow of the pulse. From equation (1), the electron density may be approximated by

$$n_e \approx \left[ \frac{W}{\sum k_{Cl} \Delta H_{Cl} n_g y_{Cl} + \sum k_{Cl_2} \Delta H_{Cl_2} n_g y_{Cl_2}} \right] \quad (18)$$

where the first term in the denominator represents losses due to e-Cl collisions and the second term represents losses due to e-Cl<sub>2</sub> collisions;  $W$  is the input power density;  $n_g$  is the total neutral density; and  $y_{Cl}$  and  $y_{Cl_2}$  refer to the mole fractions of Cl radicals and Cl<sub>2</sub> molecules, respectively. If the denominator in equation (18) were constant, the electron density would change linearly with power. This is not the case however. An increase in the time-averaged Cl fraction favours more energy dissipation by e-Cl collisions as opposed to e-Cl<sub>2</sub> collisions. For the calculated electron temperature, however,

$$\sum k_{Cl} \Delta H_{Cl}(T_e) < \sum k_{Cl_2} \Delta H_{Cl_2}(T_e). \quad (19)$$

Consequently, more electrons are required to dissipate the same level of power by e-Cl collisions as opposed to e-Cl<sub>2</sub> collisions. Since the Cl fraction increases with power, the electron density increases superlinearly with power.

The change in electron density and neutral composition with input power directly affects the evolution of negative ions. In the afterglow, the rate of decay of electron density due to dissociative attachment decreases at higher input powers due to the lower fraction of Cl<sub>2</sub> molecules. The time lag for the negative-ion flux to reach the walls, therefore, uniformly increases as the power level is increased (figure 6(c)). The maximum value of the negative-ion flux also increases with power input because there are more electrons available to be converted to negative ions in the afterglow.

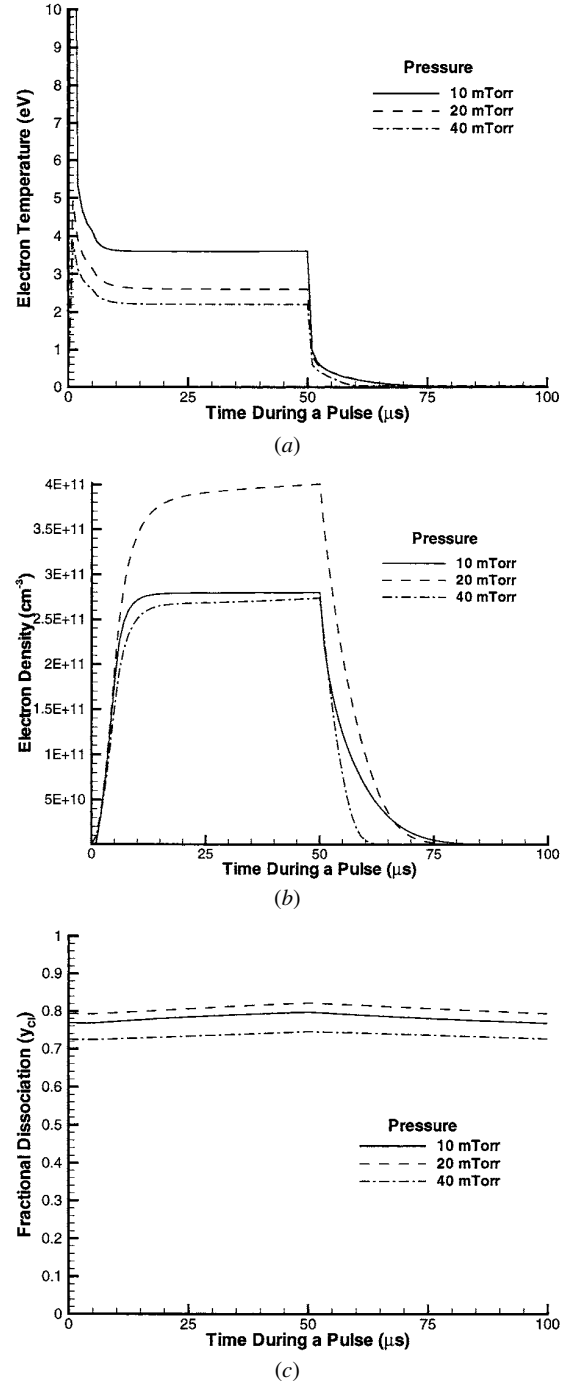


**Figure 7.** Effect of pressure on the evolution of: (a) the electron temperature, (b) the electron density, (c) the Cl mole fraction and (d) the negative-ion flux at the walls. The other conditions are at their base values (table 2).

**3.6.2. Pressure.** In contrast to power, changing the pressure results in a significant change in the electron temperature during the active glow (figure 7(a)). The electron temperature is determined by the electron continuity equation (equation (2)) which may be written approximately as

$$(k_{ioniz}(T_e) - k_{attach}(T_e))n_g(p) \approx \frac{D_{eff}(T_e, p)}{L^2}. \quad (20)$$

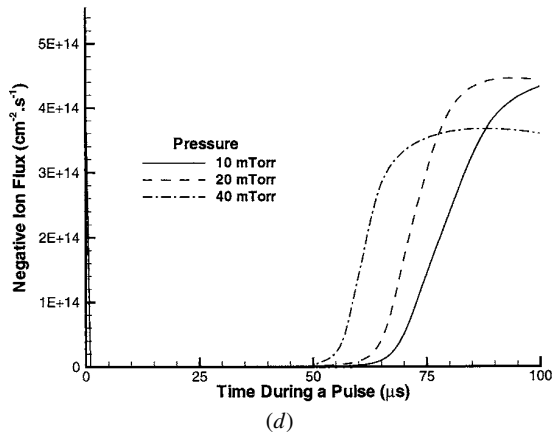


Figure 7. (Continued)

That is, the net production of electrons is balanced by ambipolar diffusion losses to the walls. As the operating pressure is lowered, the effective diffusion coefficient ( $D_{eff}$ ) increases while the neutral density ( $n_g$ ) decreases, favouring a decrease in the rate of production of electrons. Therefore, higher electron temperatures are required to compensate for greater diffusion losses and lower neutral densities as the operating pressure is lowered. A similar dependence of electron temperature on pressure was obtained experimentally by Malyshev *et al* [24, 25].

The changing electron temperature causes a non-monotonic variation in the plateau value of electron density at different pressures (figure 7(b)). From equation (18), the quasi-steady value of electron density may be expressed as

$$n_e \approx \left[ \frac{W}{\sum_i k_i(T_e) \Delta H_i n_g(p)} \right]. \quad (21)$$

The electron temperature is higher at lower pressures resulting in higher rate coefficients  $k_i$  for the dissipation of electron energy by inelastic collisions. Therefore, a relatively lower number of electrons are required to dissipate the same power. As the electron temperature decreases with increasing pressure, the rate coefficients decrease and more electrons are required to dissipate the power. At even higher pressures, however, the increase in the neutral density ( $n_g$ ) begins to dominate over the effect of temperature and a lower number of electrons are required to dissipate the same input power. The plateau value of electron density, therefore, first increases and then decreases with increasing pressure.

This non-monotonic behaviour in electron density results in a neutral composition that is relatively insensitive to the pressure (figure 7(c)). The Cl fraction initially increases with pressure due to a decrease in diffusion losses to the walls. The electron temperature, however, also drops as the pressure is increased and eventually causes a decrease in the rate of production of Cl radicals. The Cl radical density, therefore, first increases slightly and then decreases as the pressure is increased.

The time lag in the afterglow before negative ions reach the walls is a function of the rate of decay of the electron density. Since the neutral composition remains relatively constant as a function of pressure, the rate of dissociative

attachment of electrons increases uniformly with neutral density as the pressure is increased. Therefore, the time lag before the negative-ion flux reaches the walls uniformly decreases with increasing operating pressure (figure 7(d)).

While the loss of electrons by dissociative attachment increases with increasing pressure, the loss by ambipolar diffusion decreases. Therefore, a greater fraction of electrons is converted to negative ions in the afterglow and the negative-ion density increases at higher pressures. The magnitude of the flux of negative ions, however, also depends on the ion diffusivity, which decreases with pressure. Therefore, the peak value of the negative-ion wall flux initially increases as the pressure is increased, but then drops (figure 7(d)). For a pressure of 10 mTorr, the time lag for the formation of an ion-ion plasma is too long for the negative-ion flux to reach a peak within the 50  $\mu$ s afterglow period.

**3.6.3. Duty ratio.** Another important operating variable available in pulsed-power operation is the duty ratio i.e. the fraction of the period during which power is 'on'. For a fixed peak power level, the predicted effects of increasing the duty ratio are equivalent to changing the time-averaged power. Higher duty ratios result in greater dissociation of Cl<sub>2</sub> molecules during the transient phase of plasma ignition. This increase stems from the longer time available for dissociation within each pulse as the duty ratio is increased. This is different from the effect of increasing the peak power input (at a fixed duty ratio) itself, in which case more dissociation occurs due to the presence of higher electron densities. Higher electron densities, in turn, result in a faster rate of dissociation at higher power levels. Nevertheless, the predicted value of Cl density at the periodic steady state responds only to the time-averaged value of power input and increases monotonically as the duty ratio is increased (figure 8(b)).

The increase in the Cl fraction with duty ratio causes more electron energy to be dissipated by Cl excitations as opposed to Cl<sub>2</sub> excitations. As in the case of varying the peak power, equations (18) and (19) show that more electrons are required to dissipate the same amount of power by Cl excitations as opposed to Cl<sub>2</sub> excitations. Therefore, the quasi-steady value of electron density increases monotonically with an increasing duty ratio (figure 8(a)).

The rate of electron attachment in the afterglow decreases as the Cl fraction increases. Consequently, the time lag for the negative-ion flux to reach the walls uniformly increases as the duty ratio is increased (figure 8(c)). The magnitude of the negative-ion flux scales with the negative-ion density in the afterglow and decreases as the duty ratio is increased.

Experimental results [23] show a more complicated behaviour. The quasi-steady value of the electron density shows a non-monotonic trend with the duty ratio; the electron density initially increases as the duty ratio increases, attains a maximum and then steadily decreases for higher duty ratios. Lower electron densities for higher duty ratios reduce the rate of dissociation of Cl<sub>2</sub> during the transient period of plasma ignition. Therefore, the Cl fraction at the periodic steady state is expected to be relatively insensitive to the duty ratio.

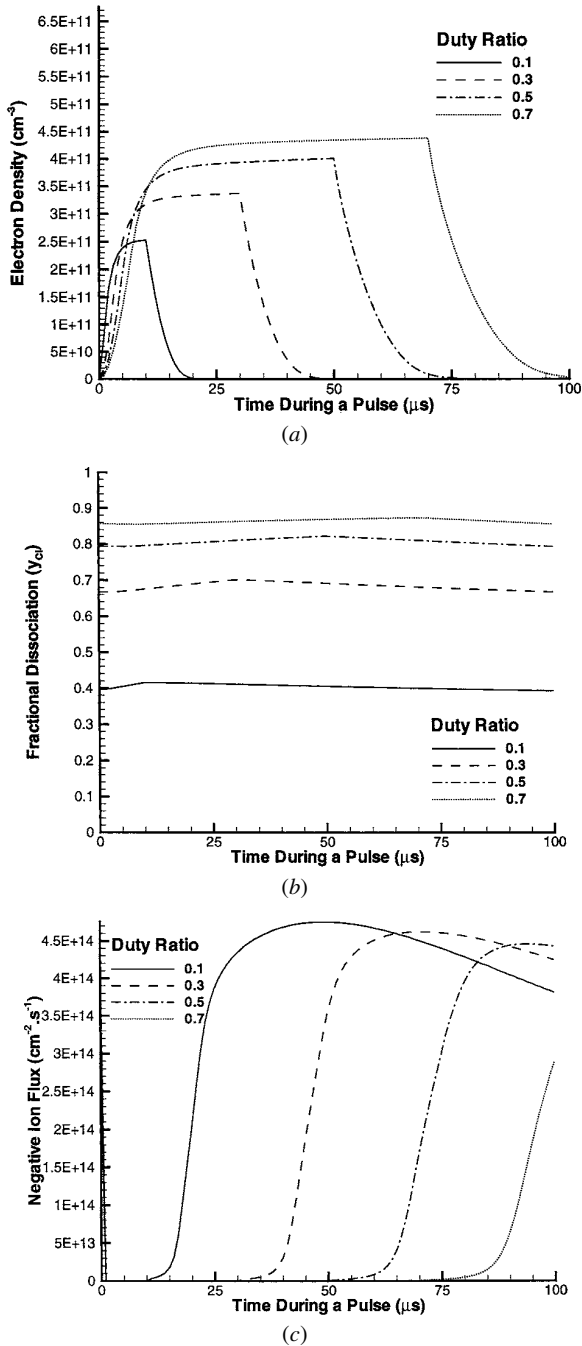


**Figure 8.** Effect of duty ratio on the evolution of: (a) the electron density, (b) the Cl mole fraction and (c) the negative-ion flux at the walls. The other conditions are at their base values (table 2).

This is evident from the experimental results, which show that the rate of decay of electrons in the afterglow remains unchanged as the duty ratio is increased, indicating that the rate of dissociative attachment is also relatively constant.

The non-monotonic behaviour of the electron density with the duty ratio suggests a change in the quasi-steady value of the electron temperature. This is also evident from the experimental results, which show that the electron density increases with different slopes during the early active glow for different duty-ratios. In the model, however, the electron temperature is governed by the electron continuity

equation and requires that the production of electrons by ionization is balanced by losses due to ambipolar diffusion and dissociative attachment (equation (20)). As the Cl fraction increases in the transient phase, there is a decrease in the attachment rate and a shift of production of electrons from molecular ionization to atomic ionization. However, the contribution of dissociative attachment is small in the active glow and the difference in the threshold energies of molecular and atomic ionization is only 1.5 eV. For  $T_e$  values much greater than 1.5 eV, the electron temperature predicted by the model (not shown) becomes insensitive to changes in the Cl fraction. The final result is that the predicted electron density monotonically increases on increasing the duty ratio.

**3.6.4. Pulse period.** For a fixed duty ratio, the time-averaged value of power remains constant as the pulse period is increased. Therefore, the average Cl fraction predicted by the model does not increase significantly as the pulse period is increased (figure 9(b)). Only the small modulation of the Cl density within each pulse increases as the pulse period is increased.

Since the neutral composition remains constant, the electron density and electron temperature approach the same quasi-steady values as the pulse period is increased (figure 9(a)). Similarly, the rate of decay of the electrons by dissociative attachment in the afterglow is insensitive to the pulse period. For short periods, however, there is insufficient time for the electron density to decay enough for the electrostatic fields to collapse in the afterglow. Therefore, a minimum time period is required for the formation of an ion-ion plasma in the afterglow. Beyond this minimum time period, the time lag before the negative-ion flux reaches the walls remains constant (figure 9(c)). Similarly, the magnitude of the peak of the negative-ion flux is insensitive to the pulse period and larger pulse periods may be used to improve the fraction of time an ion-ion plasma is sustained in the reactor.

Experimental results [23], show a more complicated dependence on pulse period. The peak electron density initially decreases as the pulse period is increased and then increases with a further increase in the pulse period. The rate of decay of electron density decreases uniformly as the pulse period is increased, indicating a decrease in the rate of attachment and Cl<sub>2</sub> density. This suggests that the time lag for the formation of an ion-ion plasma also increases as the pulse period is increased.

#### 4. Limitations of the model

The overall features predicted by the model (see figures 1(a), 1(c), 3, 5, 6(a) and 7(a)) have been confirmed experimentally [2, 23–25, 30]. However, some disparities exist between experimental [23] and predicted effects of the duty ratio and pulse period on the peak electron density in the active glow. These disparities may suggest some limitations in the model that must be improved to obtain a better agreement with experiments.

First, the plasma is ignited in the early active glow in the presence of only a few electrons. At this low electron density, the electrical conductivity of the plasma is too low

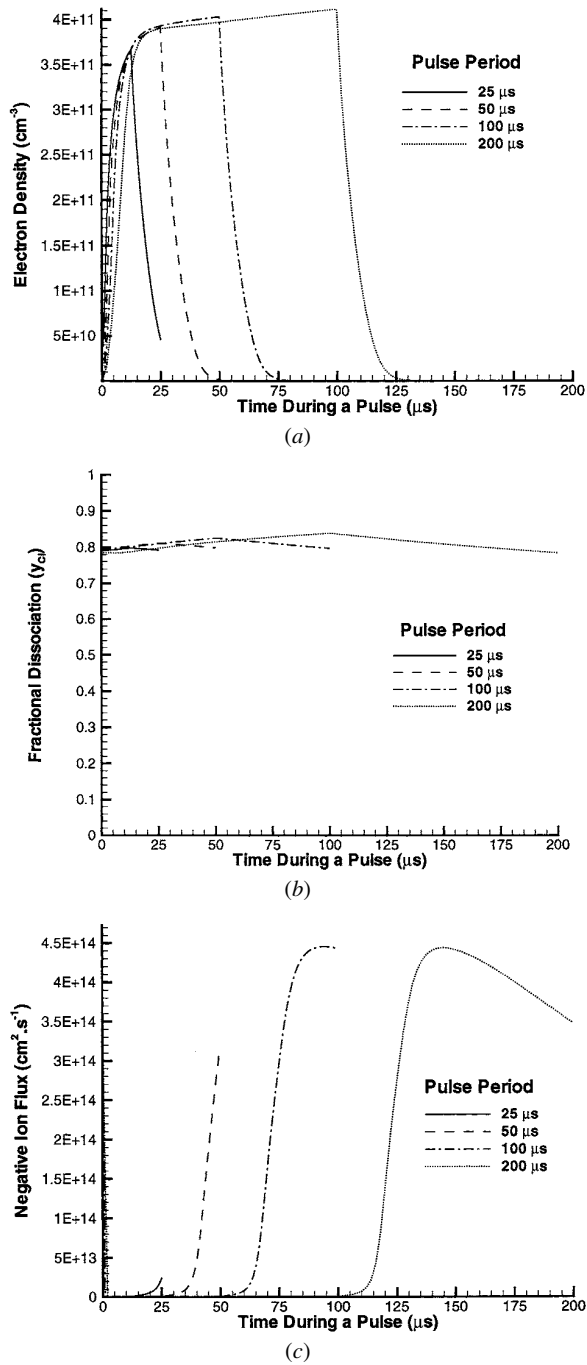


**Figure 9.** Effect of pulse period on the evolution of: (a) the electron density, (b) the Cl mole fraction, (c) the negative-ion flux at the walls. The other conditions are at their base values (table 2).

to be ignited directly in the inductive mode. Experiments [23] show that the plasma first ignites due to the capacitive coupling with the induction coil. Only after a sufficient electron density is built up in the reactor does the transition from the capacitive mode to the inductive mode occur in the experiments. In the model, however, the total power input is assumed to be constant and this transition from capacitive to inductive heating in the early active glow is not modelled.

Second, the assumption of a Maxwellian electron energy distribution may not be suitable especially for low electron densities in the early active glow. In many cases, high values

of the electron temperature are predicted during the early spike, which may not be physically plausible.

Furthermore, the model is only one dimensional in nature, whereas most experimental configurations require at least a 2D description. Power input from the induction coil is expected to peak near the coils and the negative-ion density may peak off-centre. Dead regions of the reactor (receiving little power directly from the power source) may harbour a significant number of negative ions and undissociated  $\text{Cl}_2$  molecules which may also effect the evolution of the plasma.

Finally, secondary electron emission has been neglected because the effect of bias is not studied in this paper. Secondary electrons may destroy the ion-ion plasma state formed late in the afterglow. However, due to the absence of significant electrostatic fields, any secondaries produced should quickly escape the plasma by free diffusion. For example, Ahn *et al* [2] applied a bias in the afterglow, but the measured electron density continued to drop exponentially in the afterglow, i.e. there was no apparent accumulation of electrons due to secondary electron emission or other sources.

## 5. Conclusions

A 1D fluid model for pulsed (square-wave power modulated) chlorine discharges was developed. It was shown that the negative-ion density profiles change significantly during the pulse. Self-sharpening negative-ion fronts are formed due to the electrostatic fields in the active glow, which squeeze negative ions into the core of the discharge. Negative ions are trapped in the core by an electropositive edge plasma and there is no flux of negative ions to the walls. The electron density decays in the afterglow due to dissociative attachment and ambipolar diffusion to the walls. There is an abrupt transition from an electron-dominated plasma to an ion-ion plasma in the afterglow. The ion-ion plasma is characterized by vanishingly weak electrostatic fields and free diffusion of negative (and positive) ions to the walls. The formation of an ion-ion plasma in the afterglow is favoured at lower power levels, higher pressures, and lower duty ratios. A minimum afterglow time is required for an ion-ion plasma to form and the negative ions to reach the walls. Increasing the afterglow period increases the fraction of time an ion-ion plasma is sustained in the reactor.

The model predicted complex spatio-temporal negative-ion density profiles. At the centre of the discharge, the negative-ion density increases during the power 'on' stage of the pulse and decreases during the power 'off' stage of the pulse. At off-axis locations, however, the time evolution is more complex. Specifically, the negative-ion density goes through peak values during both the power 'on' and the power 'off' stages of the pulse. This is due to the moving negative ion density fronts mentioned above. Both experimental and model results show that the increase in the plateau value of electron density during a pulse is not linear with power input. This is due to changing the neutral composition (more molecular dissociation) as the peak power level is increased.

Although the overall trends predicted by the model show good agreement with experimental results, the effect of duty ratio and pulse period on the electron density is not captured adequately. Multidimensional modelling studies

that include a more detailed description of power input from the coils (including capacitive coupling) and a calculation of the electron energy distribution (and its deviation from Maxwellian during the early stages of the active glow) should be able to show even better agreement with data. Similarly, further experiments are encouraged to validate important trends predicted by the model which have not yet been measured. An example is the time evolution of the fluxes of positive and negative ions bombarding the walls of the reactor.

## Acknowledgments

We thank the National Science Foundation (CTS-9713262) and the State of Texas (Texas Advanced Technology Program) for financial support. Many thanks to Drs I D Kaganovich, L J Overzet, M L Malyshev and G A Hebner for helpful technical discussions throughout this work.

## References

- [1] Samukawa S and Mieno T 1996 *Plasma Sources Sci. Technol.* **5** 132
- [2] Ahn T H, Nakurama K and Sugai H 1996 *Plasma Sources Sci. Technol.* **5** 139
- [3] Shibayama T, Shindo H and Horiike Y 1996 *Plasma Sources Sci. Technol.* **5** 254
- [4] Kinoshita T, Hane M and McVittie J 1996 *J. Vac. Sci. Technol. B* **14** 560
- [5] Hwang G S and Giapis K P 1997 *J. Vac. Sci. Technol. B* **15** 70
- [6] Arnold J C and Sawin H H 1991 *J. Appl. Phys.* **70** 5314
- [7] Sugai H, Nakamura K, Hikusaka Y and Nakamura M 1995 *J. Vac. Sci. Technol. A* **13** 887
- [8] Boswell R and Porteous R 1987 *J. Appl. Phys.* **62** 3123
- [9] Verdeyen J, Bederman J and Overzet L 1990 *J. Vac. Sci. Technol. A* **8** 1851
- [10] Jiang P, Economou D J and Shin C B 1995 *Plasma Chem. Plasma Process.* **15** 383
- [11] Park S-K and Economou D J 1991 *J. Electrochem. Soc.* **138** 1499
- [12] Meyyappan M 1996 *J. Vac. Sci. Technol. A* **14** 2122
- [13] Ashida S and Lieberman M A 1997 *Japan. J. Appl. Phys.* **36** 854–61
- [14] Lymberopoulos D P, Kolobov V I and Economou D J 1998 *J. Vac. Sci. Technol. A* **16** 564
- [15] Overzet L J, Lin Y and Luo L 1992 *J. Appl. Phys.* **72** 5579
- [16] Lymberopoulos D P and Economou D J 1995 *J. Res. Natl. Inst. Stand. Technol.* **100** 473
- [17] Kouznetsov I, Litchenberg A J and Lieberman M A 1999 *J. Appl. Phys.* **86** 4142
- [18] Kolobov V I and Economou D J 1998 *Appl. Phys. Lett.* **72** 656
- [19] Rogoff G L 1985 *J. Phys. D: Appl. Phys.* **18** 1533
- [20] Kaganovich I D, Economou D J, Ramamurthi B N and Midha V 2000 *Phys. Rev. Lett.* **84** 1918
- [21] Kaganovich I D and Economou D J 2000 *Phys. Rev. E* at press
- [22] Midha V and Economou D J 1998 *45th Int. Symp., American Vacuum Soc. (Baltimore, MD, November 2–6 1998)*
- [23] Hindmarsh A C 1983 *Scientific Computing* ed R S Stepleman (IMACS) (Amsterdam: North-Holland) p 55
- [24] Lymberopoulos D P and Economou D J 1997 *IEEE Trans. Plasma Sci.* **23** 573
- [25] Hebner G A and Fleddermann C B 1997 *J. Appl. Phys.* **82** 2814–21
- [26] Malyshev M V, Donnelly V M, Colonell J I and Samukawa S 1998 *45th Int. Symp., American Vacuum Soc. (Baltimore, MD, November 2–6, 1998)*
- [27] Malyshev M V 1999 *PhD Dissertation* Princeton University
- [28] Kaganovich I D and Tsendin L D 1993 *Plasma Phys. Rep.* **19** 645
- [29] Tsendin L D 1989 *Sov. Phys.–Tech. Phys.* **34** 11
- [30] Litchenberg A J, Vahedi V, Lieberman M A and Rognlien T 1994 *J. Appl. Phys.* **75** 2339
- [31] Christophorou L G and Olthoff J K 1999 *J. Phys. Chem. Ref. Data* **28** 131
- [32] Smith D, Dean A G and Adams N G 1974 *J. Phys. D: Appl. Phys.* **7** 1944